Enhancement of the Leading-Edge Separation Vortices by Trailing-Edge Lateral Blowing

Koji Miyaji*
University of Tokyo, Tokyo 113, Japan
and
Kozo Fujii† and Keiichi Karashima‡
Institute for Space and Astronautical Science, Kanagawa 229, Japan

Introduction

A PRIMARY feature of the flow over the leeward side of the delta wing is a leading-edge separation vortex. It modifies the potential flow region and induces the suction peak beneath the vortex axis. At a high angle of attack, the spiral-shaped vortices emanating from the leading edge begin to break down near the trailing edge. This causes lift stall, and asymmetrical vortices above the right and the left wings generate unexpected rolling moment and create lateral instability. One solution to this problem may be to set up a strake or a canard wing. Another method is a dynamic control of the flowfield instead of changing the planform of the wing. Various types of the blowing have been suggested under this concept. A blowing slot was opened on the fuselage, near the leading edge of the root chord, and the jet was injected toward the vortex core to supply momentum for the vortex.[1] In other research, a slit was opened along the leading edge of the wing, and the jet was injected in the spanwise[2] or tangential direction.[3] It is reported that the spanwise blowing strengthens the leading-edge separation vortex at prestall angles, and the tangential blowing restores the vortical flowfield in the poststall regime. Although each blowing has its own effect, it commonly aims at controlling the strength of the vortex, and the blowing slot is set near the leading edge. A totally different blowing concept was suggested elsewhere.[4,5] The flowfield, including the blowing, is shown schematically in Fig. 1. The jet is injected under the trailing edge in the outboard direction. The previous research[4,5] reported some advantages over other blowings, that is, larger increase of the lift and delay of the stall angle to a higher angle of attack. However, precise information was not available in the experiment, and the physical mechanism was not clarified. In the present Note, the flow around a delta wing, including the trailing-edge lateral blowing, is numerically simulated, and the mechanism of the change of the flowfield induced by the blowing is clarified.

Flow Configuration and Numerical Approach

The wing considered here has a 12% circular-arc chordwise section. The planform of the wing is a trapezoid with 45-deg-swept angle at the leading edge and a 0-deg-swept angle at the trailing edge. This Note focuses on the effects of the blowing at various angles of attack. The freestream Mach number is 0.3, the Reynolds number is 10^6, and the angle of attack is varied. The nondimensional blowing momentum coefficient C_μ, defined later, is also fixed at 0.076, which is the maximum value used in the experiment.

The governing equations are the three-dimensional thin-layer Navier–Stokes equations. The convective terms are discretized with the flux difference-splitting by Roe,[6] and the MUSCL interpolation is used for the higher-order extension. The time-integration algorithm is the LU-ADI factorization method.[7] Because the leading-edge sweep angle of 45 deg is small, the potential flow region near the centerline of the wing is much larger than that of the delta wing with a large sweep angle. Therefore, the leading-edge separation vortex may be much weaker. For this type of flow conditions, the boundary-layer separation in the potential region should be predicted accurately in addition to the leading-edge separation vortex. The turbulence model of Baldwin–Lomax is modified to search the vorticity only within the boundary layer and is used to avoid large unphysical turbulent viscosity.

The grid topology is C-type in the chordwise direction and H-type in the spanwise direction. The number of grid points is 161 in the chordwise direction (ξ direction), 61 in the spanwise direction (η direction), and 35 in the normal direction (ζ direction), resulting in 343,735 points. The computational grid corresponds to the medium or the fine grid of Fujii et al.,[8] and the resolution of the grid is considered to be adequate to capture the leading-edge separation vortex. Furthermore, to increase the number of grid points around the blowing slot, a secondary overset grid, which is four times finer in the ξ direction and two times finer in ζ direction than the global grid, is prepared around the slot. The number of grid points of the subgrid is about 140,000. Although rectangular cells are used, the locally fine grid covers the jet slot with sufficient grid points. The Fortified Solution Algorithm (FSA) zonal scheme[9] is used for the information exchange at the interfaces between the global grid and the local grid.

The boundary conditions are summarized as follows: The symmetry plane of the wing is treated as a viscous wall because a half-cut wing model was attached to the sidewall of a wind tunnel in the experiment. In the preliminary computations preceding these results, the sidewall was treated as a slip wall. The results showed some nonnegligible discrepancies from the experimental results, and it has turned out that the viscous effects of the sidewall have large effects on the leading-edge separation vortices over the delta wing. Assuming that the boundary layer grows from the exit of the plenum chamber, the thickness of the turbulent boundary layer is determined by the subsequent formula, and the velocity profile is determined by the one-seventh power law[10]:

$$\delta(x) = 0.37x(U_\infty x/\nu)^{-\frac{1}{5}}, \qquad u/U_\infty = [y/\delta(x)]^{\frac{1}{7}}$$

The jet slot is located in the symmetry plane. At the grid points covering the blowing slot, the pressure and the density are determined by assuming that the air expands isentropically from the stagnation condition at the plenum chamber to the jet exit. A sonic jet is assumed because the stagnation pressure is high enough for the flow to choke at the exit. Therefore, the jet pressure p_j and the density ρ_j are determined by subsequent formulas:

$$p_j = p_{0_j}[2/(\gamma+1)]^{\gamma/(\gamma-1)}, \qquad \rho_j = \rho_{0_j}[2/(\gamma+1)]^{1/(\gamma-1)}$$

where the subscript 0_j denotes the stagnation property in the plenum chamber and γ is the ratio of the specific-heat constant. The velocity profile at the exit is prescribed to be parabolic. The nondimensional

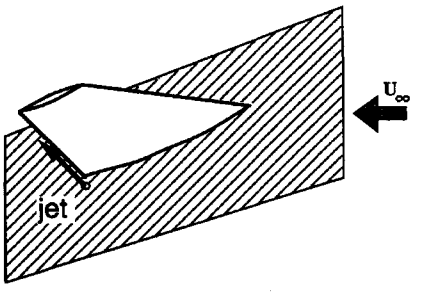

Fig. 1 Schematic of the trailing-edge lateral blowing.

Presented as Paper 94-0181 at the AIAA 32nd Aerospace Sciences Meeting, Reno, NV, Jan. 10–13, 1994; received April 13, 1995; revision received March 29, 1996; accepted for publication April 22, 1996.

*Graduate Student, Department of Aerospace Engineering, Hongo 7-3-1, Bunkyo-ku. Member AIAA.
†Associate Professor, Yoshinodai 3-1-1, Sagamihara. Associate Fellow AIAA.
‡Professor, Yoshinodai 3-1-1, Sagamihara. Member AIAA.

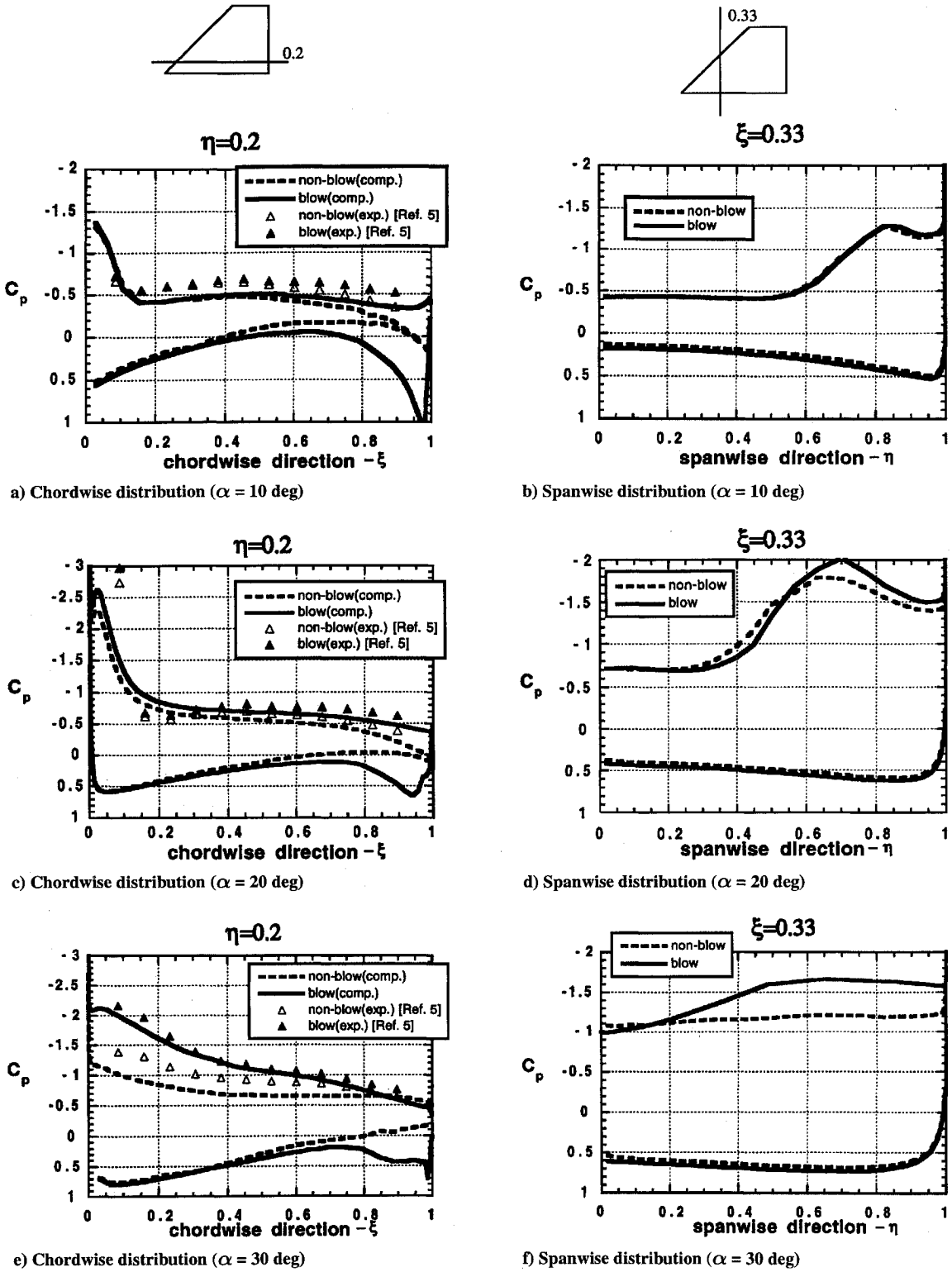

a) Chordwise distribution (α = 10 deg)

b) Spanwise distribution (α = 10 deg)

c) Chordwise distribution (α = 20 deg)

d) Spanwise distribution (α = 20 deg)

e) Chordwise distribution (α = 30 deg)

f) Spanwise distribution (α = 30 deg)

Fig. 2 C_p distributions on the wing surface (C_μ = 0.076).

blowing coefficient C_μ, indicating the intensity of the blowing, is defined as

$$C_\mu = \frac{\int\int_{A_j} \rho_j V_j V_j \cdot \mathrm{d}A_j}{q_\infty S_{\text{wing}}}$$

where subscript j denotes the property at the jet exit. The numerator is the total momentum injected from the blowing slot, and the denominator is the freestream dynamic pressure multiplied by the wing surface area.

Results and Discussion

Figure 2a shows the chordwise C_p distributions at 10-deg angle of attack for both the blowing and the nonblowing cases. The experimental data are available only on the upper surface. The computational results are plotted for both the upper and the lower surfaces. The computed result shows qualitative agreement on the blowing effect with the experimental result. The pressure hardly changes near the leading edge but decreases on the upper surface and increases on the lower surface near the trailing edge. Both result in the lift increase, as discussed later. Figure 2b shows the spanwise

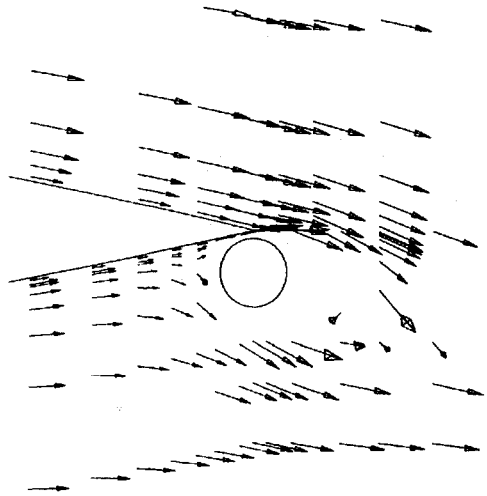

Fig. 3 Velocity vector plots around the jet core.

C_p distributions at the same angle of attack. The negative C_p peak near $\eta = 0.8$ is attributable to the leading-edge separation vortex. The blowing does not change the vortex strength at this angle of attack.

Figure 3 shows velocity vectors near the jet slot. The vectors in the jet core are not plotted. The main flow is decelerated ahead of the jet core, and it shows that the jet stream works as an obstacle lying laterally against the main flow. That is why the pressure increases on the lower surface of the wing. The flow partly merges with the jet stream and partly turns around the jet core and accelerates again. Especially between the jet core and the wing surface, the velocity magnitude becomes large because the streamlines become narrow. The accelerated flow goes out from the trailing edge and induces the chordwise velocity, which results in the pressure decrease near the trailing edge on the upper surface as well.

Figures 2c and 2d show the C_p distributions at 20-deg angle of attack. The qualitative effects of the blowing are the same as the case of 10 deg, but in the chordwise C_p distribution, the low-pressure region on the upper surface of the wing extends to the front part of the wing. The effect can be seen clearly in the spanwise C_p distribution. The negative pressure peak becomes higher by the blowing and this shows that the leading-edge vortex is strengthened more by the blowing at this angle of attack.

The difference of the blowing effect between the 10-deg case and the 20-deg case can be explained as follows. At 10-deg angle of attack, the effect of the leading-edge separation vortex is limited only near the leading-edge part. The trailing edge is covered by the potential flow. At 20 deg, the leading-edge vortex is stronger, and the vortex core moves toward the root chord. Because the jet reaches almost the same distance from the slot, independently on the angle of attack, the jet can affect the vortical flow region at 20-deg angle of attack.

Figures 2e and 2f show the C_p distributions at 30-deg angle of attack. The C_p distribution for the nonblowing case becomes almost constant, and it indicates that the leading-edge vortex has broken down at the 20% spanwise station. The blowing causes a drastic effect as observed both in the experiment and in the computation. In the chordwise C_p distribution, the pressure on the upper surface becomes much lower near the leading edge. As a result, the slope of the C_p distribution appears near the leading edge. A similar effect can be seen in the spanwise C_p distribution. A minimum C_p appears instead of the flat profile for the nonblowing case. These C_p distributions show that the leading-edge vortex recovers by the blowing.

Figure 4 shows the C_L-α curve for the nonblowing case and the blowing case. The lift increase attributable to the blowing is apparent. Because the blowing increases the lift on both the upper and the lower surfaces, the increment is fairly large. With the blowing, the maximum lift increases, and the stall angle is increased by about 5 deg as well. The lift increase becomes larger up to 30-deg angle of attack. At 10 deg, the blowing modifies the pressure only near

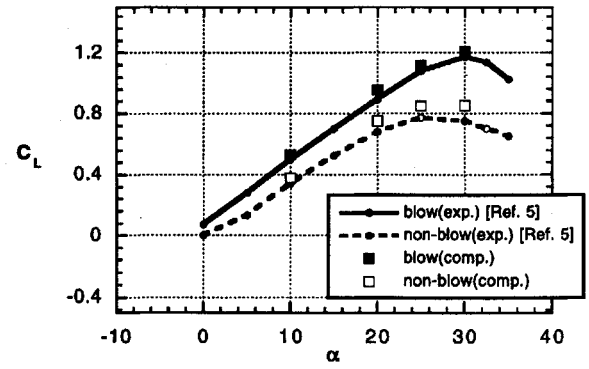

Fig. 4 C_L-α curve: effect of the blowing.

the trailing edge. At 20 deg, the blowing strengthens the leading-edge separation vortices and the suction peak become higher near the leading edge. This additional pressure modification makes the lift increase larger. Furthermore, at 30-deg angle of attack, the lift increases more because the leading-edge separation vortices recover. At higher angles of attack, the increment of the lift decreases in the experiment, and it is imagined that the vortex breakdown cannot be prevented even with the blowing. Although the drag also increases by the blowing, the increment is much smaller than the lift increase. The modification of the pressure distribution of the wing mainly increases the normal force (z direction of the body axis).

Conclusions

The numerical simulations were carried out for the study of trailing-edge lateral blowing for the delta wing. The blowing decreases the pressure on the upper surface and increases the pressure on the lower surface, but the effect is somewhat different at each angle of attack. At low angles of attack, the blowing modifies the pressure only in the potential flow region. At moderately high angles of attack, the induced lower pressure affects the leading-edge separation vortex over the wing. The vortex is strengthened by the blowing. At higher angles of attack where the vortex breakdown occurs, the blowing helps the leading-edge separation vortex to recover. The breakdown is delayed.

The blowing increases both the lift and the drag, but the increase of the lift is much larger than that of the drag. Therefore, the blowing improves the lift/drag ratio.

References

[1]Bradley, R. G., and Wray, W. O., "A Conceptual Study of Leading-Edge-Vortex Enhancement by Blowing," *Journal of Aircraft*, Vol. 11, No. 1, 1974, pp. 33–38.

[2]Yeh, D. T., Tavella, D. A., Roberts, L., and Fujii, K., "Navier–Stokes Computation of the Flow Field over Delta Wings with Spanwise Leading Edge Blowing," AIAA Paper 88-2558, June 1988.

[3]Yeh, D. T., Tavella, D. A., Roberts, L., and Fujii, K., "Numerical Study of the Effect of Tangential Leading Edge Blowing on Delta Wing Vortical Flow," AIAA Paper 89-0341, Jan. 1989.

[4]Karashima, K., and Sato, K., "The Effect of Lateral Blowing on Aerodynamic Characteristics of Low Aspect Ratio Wings," *Journal of the Japan Society for Aeronautical and Space Sciences*, Vol. 37, No. 425, 1983, pp. 14–20 (in Japanese).

[5]Karashima, K., Sato, K., Tanikatsu, T., and Yamaguchi, Y., "The Effect of Lateral Blowing on Aerodynamic Characteristics of Low Aspect Ratio Wings," *Proceedings of the 30th Aircraft Symposium*, Tsukuba, Ibaraki, Japan, 1992, pp. 156–159 (in Japanese).

[6]Roe, P. L., "Characteristic-Based Schemes for the Euler Equations," *Annual Review of Fluid Mechanics*, Vol. 18, 1986, pp. 337–365.

[7]Obayashi, S., Matsushima, K., Fujii, K., and Kuwahara, K., "Improvement in Efficiency and Reliability for Navier–Stokes Computations Using the LU-ADI Factorization Algorithms," AIAA Paper 86-338, Jan. 1986.

[8]Fujii, K., Gavali, S., and Holst, T. L., "Evaluation of Navier–Stokes and Euler Solutions for Leading-Edge Separation Vortices," NASA TM 89458, June 1987.

[9]Fujii, K., "Unified Zonal Method Based on the Fortified Solution Algorithm," *Journal of Computational Physics*, Vol. 118, No. 1, 1995, pp. 92–108.

[10]Schlichting, H., *Boundary-Layer Theory*, McGraw–Hill, New York, pp. 637, 638.